Uptake of Gas-Phase SO_2, H_2S, and CO_2 by Aqueous Solutions

J. Boniface, Q. Shi, Y. Q. Li, J. L. Cheung, O. V. Rattigan, and P. Davidovits*

Department of Chemistry, Merkert Chemistry Center, Boston College, Chestnut Hill, Massachusetts 02467-3809

D. R. Worsnop, J. T. Jayne, and C. E. Kolb

Center for Aerosol and Cloud Chemistry, Aerodyne Research Inc., Billerica, Massachusetts 01821-3976

Received: February 7, 2000; In Final Form: May 22, 2000

The uptake of gas-phase SO_2, H_2S, and CO_2 by aqueous solutions was studied as a function of pH and temperature using droplet train flow reactor and bubble train reactor apparatuses. All three atmospheric species react with H_2O and OH^-, acidifying aqueous solutions. Studies yielded the reaction rates of SO_2, H_2S, and CO_2 with OH^- and the mass accommodation coefficient (α) of SO_2 on water as a function of temperature. The second-order aqueous-phase rate coefficients at 291 K for SO_2, H_2S and CO_2 reaction with OH^- are $(1.1 \pm 0.2) \times 10^{10}$, $(1.7 \pm 0.2) \times 10^9$, and $(4.0 \pm 0.7) \times 10^3$ M^{-1} s^{-1}, respectively. As far as we can determine, the rate coefficients for SO_2 and H_2S have been determined here for the first time. At 291 K, for SO_2, $\alpha = 0.175 \pm 0.015$, and as in previous studies, the temperature dependence of α is well represented by the relationship $\alpha/(1-\alpha) = \exp(-\Delta G_{obs}/RT)$ with $\Delta H_{obs} = -7.6 \pm 0.6$ kcal mol^{-1} and $\Delta S_{obs} = -29.2 \pm 2.1$ cal mol^{-1} K^{-1}.

Introduction

In this work, we describe uptake studies of gas-phase SO_2, H_2S, and CO_2 by aqueous solutions as a function of pH and temperature. These three atmospheric species exhibit similar chemical behaviors that contribute to the acidification of aqueous media in the atmosphere. Sulfur dioxide oxidation is responsible for about 90% of atmospheric H_2SO_4, and an estimated 50% of this oxidation occurs via heterogeneous reactions.[1] Hydrogen sulfide is a major biogenic reduced sulfur species, emitted into the atmosphere by vegetation, soils, and marine waters,[2] that is oxidized by the OH radical in the gas phase to produce SO_2.[3] H_2S may also be important to O_3 chemistry, as in the aqueous phase, H_2S dissociates readily to HS^-, which, in turn, reacts rapidly with O_3.[4] Of the three gas-phase species, CO_2 is the least reactive but perhaps the most atmospherically important. Because of its high atmospheric abundance (~370 ppm) and its infrared absorption properties, CO_2 plays an important role in the global warming process.

The pH-dependent reactions of SO_2 and CO_2 in aqueous solution are ($R = SO_2$ or CO_2)

$$R(aq) + 2H_2O \underset{k_{-1}}{\overset{k_1}{\rightleftharpoons}} ROH^- + H_3O^+ \qquad (R1)$$

$$R(aq) + OH^- \underset{k_{-2}}{\overset{k_2}{\rightleftharpoons}} ROH^- \qquad (R2)$$

The pH-dependent reactions of H_2S are

$$H_2S(aq) + H_2O \underset{k_{-1}}{\overset{k_1}{\rightleftharpoons}} HS^- + H_3O^+ \qquad (R3)$$

$$H_2S(aq) + OH^- \underset{k_{-2}}{\overset{k_2}{\rightleftharpoons}} HS^- + H_2O \qquad (R4)$$

Here, k_1 is the pseudo-first-order reaction-rate coefficient of the species with H_2O, and k_2 is the second-order reaction-rate coefficient of the species with OH^-. As the current study makes evident, the forward reaction rates for SO_2, H_2S, and CO_2 with OH^- vary over nearly 6 orders of magnitude. The uptake coefficients vary over a similar range. Two complementary apparatuses were used to span this range of uptake coefficients: a droplet train flow reactor apparatus and a horizontal bubble train reactor apparatus. The uptake measurements yielded rate coefficients for the reaction of SO_2, H_2S, and CO_2 with OH^-, and the mass accommodation coefficient for SO_2 on water as a function of temperature.

In several previous uptake studies, the measured uptake was larger than predicted by bulk-phase parameters. Such enhanced uptake was observed among others in the following uptake studies: SO_2 at low pH (<2),[5] $ClONO_2$ uptake by HCl doped sulfuric acid,[6] $ClNO_2$ uptake by aqueous I^- solutions,[7] Cl_2 and Br_2 uptake by aqueous NaBr and NaI solutions,[8] and NH_3 uptake by sulfuric acid.[9] The enhanced uptake in these studies has been attributed to reactions specific to the gas−liquid interface. An added purpose of the present study is to determine whether surface-specific reactions are evident in the uptake of the three target species.

Background

Sulfur Dioxide. The interfacial mass transport of $SO_2(aq)$ has been studied by several research groups.[5,10−13] However, in these studies, the effects of reaction and mass accommodation were not uncoupled. The present $SO_2(g)$ uptake study was extended to higher pH and yielded, as far as we can determine, the first measurement of the rate coefficient (k_2) for the SO_2/OH^- reaction and the mass accommodation coefficient (α) as a function of temperature. In the earlier work of Jayne et al.,[5] the SO_2/OH^- reaction was omitted, and higher uptake at high pH (>10) was erroneously attributed to a surface reaction.

Hydrogen Sulfide. The uptake of H_2S by aqueous solutions (pH < 8.9) has been studied by De Bruyn et al.[14] Those

10.1021/jp000479h CCC: $19.00
Published on Web 07/20/2000

experiments yielded the Henry's law constant for water and the Setchenow coefficients for NaCl and $(NH_4)_2SO_4$ aqueous solutions. The rate coefficient (k_2) for the H_2S/OH^- reaction could not be determined from those studies. Here again, measurements at higher pH yielded, as far as we can tell, a first-time determination of this rate coefficient.

Carbon Dioxide. The CO_2/OH^- reaction is important in industrial processes such as the manufacture of sodium bicarbonate. For that reason, this reaction has been studied by several groups using a variety of techniques. Sirs[15] summarized his and other measurements with an expression for $k_2 = A \exp(-\Delta E/RT)$, where $A = 3.9 \times 10^{13}$ M^{-1} s^{-1} and $\Delta E = 13.21$ kcal mol^{-1} over the temperature range 0−40 °C. Our examination of the data used by Sirs suggests error limits on k_2 of about ±10%. Subsequently, Nijsing et al.[16] measured $k_2 = (4.7 \pm 0.7) \times 10^3$ M^{-1} s^{-1} at 293 K. This is about 15% lower than the value obtained from Sirs expression. A more recent measurement by Pocker and Bjorkquist[17] performed at 298 K, yielded $k_2 = 6 \times 10^3$ M^{-1} s^{-1}, about 25% lower than the value obtained from the Sirs equation.

These previous CO_2/OH^- measurements were performed at high CO_2 gas-phase densities, in the range $10^{17}-10^{18}$ molecules cm^{-3}. The present studies were performed at lower CO_2 densities typical of the atmosphere ($10^{15}-10^{16}$ molecules cm^{-3}). Any potential surface effects are more likely to be experimentally observed at lower densities.

Modeling Gas Uptake

The modeling of gas uptake by aqueous surfaces has been described in detail in our previous publications, most recently by Shi et al.[18] Here, we will present only a brief outline of the process.

A phenomenological description of the entry of gases into liquids is straightforward. First, the gas-phase molecule is transported to the liquid surface, usually by gas-phase diffusion. The initial entry of the species into the liquid is governed by the mass accommodation coefficient, α, which is the probability that an atom or molecule striking a liquid surface enters into the bulk liquid phase.

$$\alpha = \frac{\text{no. of molecules entering the liquid phase}}{\text{no. of molecular collisions with the liquid surface}} \quad (1)$$

In the absence of surface reactions, the mass accommodation coefficient determines the maximum flux, J, of gas into a liquid, which is given by

$$J = \frac{n_g \bar{c} \alpha}{4} \quad (2)$$

Here, n_g is the density of the trace gas phase and $\bar{c}$ is the trace gas average thermal speed.

In laboratory experiments, gas uptake by a liquid may be affected by gas-phase diffusion of the species to the liquid surface and also by solubility constraints as the species in the liquid approaches Henry's law saturation. In the latter process, a fraction of the molecules that enters the liquid evaporates back into the gas phase because of the limited solubility of the species. If the solvated species is subject to reactions in the aqueous phase, a steady-state flux of molecules into the liquid can be sustained. This steady-state flux is determined by the aqueous-phase reaction rate, k.

In experiments subject to these effects, the measured flux into a surface is expressed in terms of an experimental uptake coefficient, γ_{meas}, as

$$J = \frac{n_g \bar{c} \gamma_{meas}}{4} \quad (3)$$

The four processes (gas-phase diffusion, mass accommodation, Henry's law solubility, and chemical reactions) that affect the uptake of the species studied in this work are interrelated, and therefore, a quantitative description of the uptake process involves coupled differential equations. General solutions for such equations are not available. In special cases, however, the processes can be decoupled and expressed in terms of dimensionless conductances Γ_{diff}, α, Γ_{sol}, and Γ_{rxn} representing gas-phase diffusion, mass accommodation, Henry's law solubility constraints, and reactions, respectively.

As discussed in Shi et al.[18] and references therein, in the absence of surface reactions, γ_{meas} is expressed as

$$\frac{1}{\gamma_{meas}} = \frac{1}{\Gamma_{diff}} + \frac{1}{\alpha} + \frac{1}{\Gamma_b} \quad (4)$$

Here, Γ_b represents the conductance due to all bulk-phase processes, such as solubility and reactive loss processes, and Γ_{diff} represents gas-phase diffusion constraints. The gas-phase diffusion process in the droplet train flow apparatus (see following section) is well described by the semiempirical formulation of Fuchs and Sutugin.[19]

$$\frac{1}{\Gamma_{diff}} = \frac{0.75 + 0.283K_n}{K_n(1 + K_n)} \quad (5)$$

Here, K_n is the Knudsen number defined as $2\lambda/d_f$, where λ is the gas-phase mean free path with $\lambda = 3D_g/\bar{c}$; D_g is the gas-phase diffusion coefficient of the trace gas in the background gas; and d_f is the effective diameter of droplets for the diffusive process. It has been shown in detailed experimental studies that d_f is expressed in terms of droplet-forming orifice (d) as $d_f = (2.0 \pm 0.1)d$. This formulation is currently the most accurate way to take into account gas-phase diffusive transport to a train of moving droplets under the conditions of our experiments. A discussion of this formulation is found in Shi et al.[18]

The conductance Γ_{sol} represents the effect on gas uptake of the Henry's law solubility limitation. Γ_{sol} is time-dependent and to a good approximation, is given by[11,18,20]

$$\frac{1}{\Gamma_{sol}} = \frac{\bar{c}}{8RTH}\sqrt{\frac{\pi t}{D_l}} \quad (6)$$

where H (M atm^{-1}) is the Henry's law coefficient, D_l (cm^2 s^{-1}) is the liquid-phase diffusion coefficient, and t (s) is the gas−liquid interaction time.

The solubility of acidic gas-phase species such as SO_2, H_2S, and CO_2 is enhanced by the capacity of the liquid to hold the species in dissociated, ionized forms. This additional capacity afforded by the dissolved ions depends on the pH of the aqueous solution. The full solubility of the species is governed by an effective Henry's law coefficient (H_{eff}), which is given by[11,20]

$$H_{eff} = H\left(1 + \frac{K_{a1}}{[H^+]} + \frac{K_{a1}K_{a2}}{[H^+]^2}\right) = H + H\left(\frac{K_a}{[H^+]}\right) + H\left(\frac{K_{a1}K_{a2}}{[H^+]^2}\right) \quad (7)$$

where K_{a1} and K_{a2} are the first and second acid dissociation constants, respectively. The first term on the right-hand side is the physical solubility of the species. The second and third terms are the solubilities of the ions, for example, in the case of SO_2,

TABLE 1: Reaction Rates of SO_2, H_2S, and CO_2 with OH^- (k_2) and H_2O (k_1) and the parameters H, K_{A1} and K_{A2} at 291 K

species	k_2 (M^{-1} s^{-1})	k_1(s^{-1})	K_{a1} (M)	K_{a2} (M)	H (M atm^{-1})
SO_2	$(1.1 \pm 0.2) \times 10^{10}$	3.4×10^6 [a]	1.55×10^{-2} [c]	1.02×10^{-7} [f]	1.6[c]
H_2S	$(1.7 \pm 0.2) \times 10^9$	$<1 \times 10^4$	8.35×10^{-8} [d]	6.49×10^{-15} [e]	0.10[g]
CO_2	$(4.0 \pm 0.7) \times 10^3$	1.4×10^{-2} [b]	4.0×10^{-7} [e]	3.2×10^{-11} [e]	0.04[f]

[a] Eigen.[26] [b] Pinsent et al.[39] [c] Maahs.[27] [d] Millero.[34] [e] Perrin.[38] [f] Lide.[33] [g] De Bruyn et al.[14]

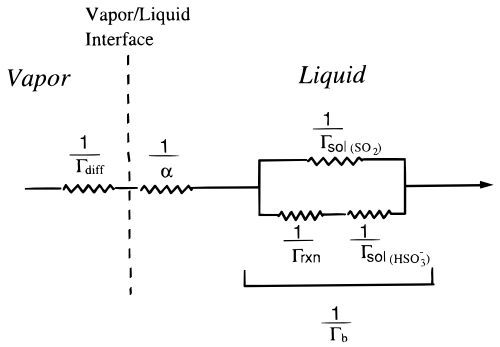

Figure 1. Electrical circuit analogue for the gas uptake process using SO_2 as an example.

HSO_3^- ($H_{HSO_3^-}$) and SO_3^{2-} ($H_{SO_3^{2-}}$). The pK_a values at 291 K are listed in Table 1.

The full solubility represented by eq 7 is not immediately available to the uptake process when the uptake is limited by the forward reaction rates k_1 and k_2 in reactions R1 and R2 and also by the hydrolysis rate of the singly charged ion. To take this into account, the solubility conductance, Γ_{sol} is divided into three parts, $\Gamma_{sol}(SO_2)$, $\Gamma_{sol}(HSO_3^-)$, and $\Gamma_{sol}(SO_3^{2-})$ representing the solubilities of SO_2, HSO_3^-, and SO_3^{2-}, for example. However, for the species studied, the third solubility does not affect the uptake. This is due to the fact that, in the pH region where the third solubility term becomes significant (i.e., pH > pK_{a2}), the uptake is limited by the forward reaction rates k_1 and k_2 and/or by the mass accommodation coefficient α. Therefore, the third solubility term can be neglected in the analysis of the uptake results.

The conductance representing the forward reaction rate is

$$\frac{1}{\Gamma_{rxn}} = \frac{\bar{c}}{4RTH\sqrt{D_l k}} \tag{8}$$

where $k = k_1 + k_2[OH^-]$ represents, in the case of SO_2 for example, the total first-order reaction rate of SO_2 to HSO_3^-. The combined effect of these conductances on uptake is represented by the resistor diagram shown in Figure 1 using SO_2 uptake as a specific example. The resistor model is described in detail most recently by Shi et al.[18] When the forward reaction rate is fast, then $\Gamma_{rxn} \gg \Gamma_{sol}(HSO_3^-)$, and uptake is limited by $\Gamma_b = \Gamma_{sol}(SO_2) + \Gamma_{sol}(HSO_3^-)$. Conversely, when $\Gamma_{rxn} \ll \Gamma_{sol}(HSO_3^-)$, then the full capacity of the liquid to hold SO_2 as HSO_3^- is not available, and uptake is limited by the forward reaction rate. In this case, $\Gamma_b = \Gamma_{sol}(SO_2) + \Gamma_{rxn}$.

The approximate expressions in eqs 6 and 8 have been shown to be in good agreement with the exact analytical solution of Danckwerts.[21] Specifically, a numerical comparison shows that eq 4 yields values of α and H each within 13% of the values obtained using the more exact formulation of Danckwerts.[21] (See Robinson et al.[22]) As is evident, with gas-phase diffusion taken into account and with values of H and D_l known, α and k can be obtained from experimentally measured uptake coefficients.

The above analysis is valid for uptake measurements obtained with the droplet train flow reactor apparatus. In the bubble train reactor apparatus, the analysis of the uptake measurements is complicated by convection currents induced by liquid motion adjacent to the bubble surface. In that case, the analysis of uptake results required more complex modeling and calibration, as described in Swartz et al.[23]

Experimental Procedures

Droplet and horizontal bubble train reactor apparatuses were used in these experiments. Both apparatuses measure the depletion of trace gas as a function of gas−liquid interaction time. The droplet train flow reactor apparatus is designed to measure uptake coefficients in the range of 5×10^{-4} to 1 for $t = 2-15$ ms. The horizontal bubble train reactor apparatus measures uptake coefficients in the range of $10^{-3}-10^{-7}$ for $t = 0.1-6$ s.

Droplet Train Flow Reactor Apparatus. In the droplet train flow reactor apparatus, pressurized liquid is passed through an orifice attached to a vibrating piezoelectric crystal to produce a train of uniform fast-moving (1500−3000 cm s^{-1}) droplets. The size of the droplets depends on the diameter of the orifice and the frequency of orifice vibration. In these experiments, the droplet diameter ranges from 150 to 300 μm. The train of aqueous droplets passes through a 30-cm-long horizontal low-pressure (6−20 Torr) flow tube, which contains the trace gas of interest at a density of about $10^{13}-10^{14}$ cm^{-3} entrained in a flowing mixture of helium and water vapor. The trace gas of interest is introduced through one of three loop injectors located along the flow tube. By selecting the gas inlet port and the droplet velocity, the gas-droplet interaction time can be varied between 2 and 15 ms. The surface area of the droplets is changed in a stepwise fashion by changing the orifice driving frequency. The density of the trace gas is monitored with a quadrupole mass spectrometer. As shown in Worsnop et al.,[11] the uptake coefficient (γ_{meas}) as defined by eq 3 is calculated from the measured change in trace gas signal via

$$\gamma_{meas} = \frac{4F_g}{\bar{c}\Delta A} \ln\frac{n_g}{n_g'} \tag{9}$$

Here, F_g is the carrier-gas volume rate of flow (cm^3 s^{-1}) through the system, $\Delta A = A_1 - A_2$ is the change in the total droplet surface area in contact with the trace gas, and n_g and n_g' are the trace gas densities at the outlet of the flow tube after exposure to droplets of areas A_2 and A_1, respectively ($n_g = n_g' + \Delta n_g$).

Horizontal Bubble Train Reactor Apparatus. In the horizontal bubble train reactor apparatus, liquid at a flow rate of 1−3 cm^3 s^{-1} is pumped through a 0.4-cm-i.d. Pyrex tube at a controlled speed of 15−35 cm s^{-1}. A low-pressure (about 50 Torr) gas flow, carrying the trace gas of interest diluted with He carrier gas, is injected into the liquid flow via a $^1/_{12}$-in. bubble injector. The experimental run begins with the bubble injector positioned 1 cm outside the flow tube, out of contact with the flowing liquid. At this point, the trace gas flows through the injector without contacting the flowing liquid and is sampled by the mass spectrometer. Then, a computer-controlled translation stage pulls the injector into the flow tube. As the injector enters the liquid, well-defined bubbles are formed, filling the diameter of the tube. The liquid flow carries the bubbles to the

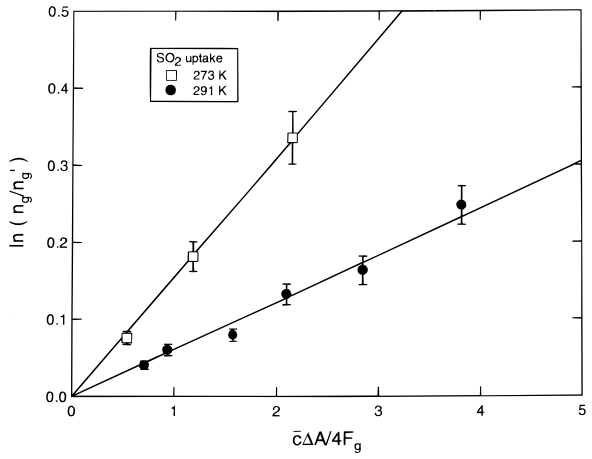

Figure 2. Plot of $\ln(n_g/n_g')$ as a function of $\bar{c}\Delta A/4F_g$ for SO_2. Droplet pH = 14, droplet temperature T = 291 K (solid circles) and 273 K (open squares). Lines are the least-squares fit to the data. The slope of the line is the measured uptake coefficient, γ_{meas} and is 0.155 ± 0.016 at 273 K and 0.061 ± 0.024 at 291 K.

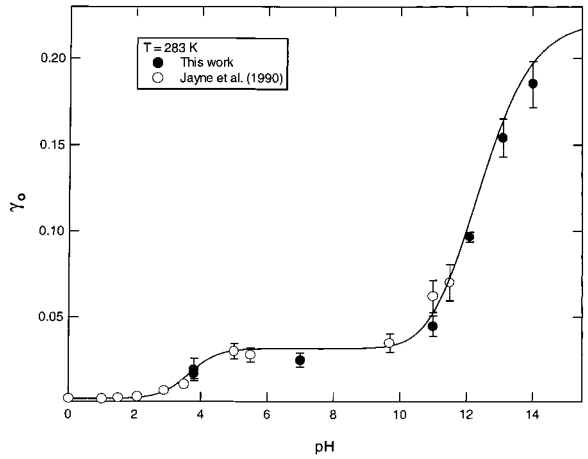

Figure 3. Uptake coefficient γ_o for SO_2 as a function of pH at 283 K. Gas−droplet contact time t = 5 ms and SO_2(g) density = 10^{14} cm^{-3}. The solid line is the global model fit to the data with α and k_2 as variables. The effect of the surface complex at low pH is included. (See text.)

end of the flow tube. The frequency, size, and speed of the bubbles are continually monitored by the light-emitting diode (LED). The position of the injector inside the tube, as well as the speed of the bubbles, defines the gas−liquid contact time. The length of the tube is 134 cm, and the gas−liquid interaction time is about 6 s. After the bubbles break at the end of the flow tube, the gas is sampled by the mass spectrometer. The signal decrease over a fixed interaction time, together with the known surface-to-volume ratio of the bubbles, determines the uptake coefficient γ_{meas}. Details of the technique are discussed in Swartz et al.[23]

The reagents SO_2 (99.9%), H_2S (99.5%), CO_2 (99.8%), and the reference gas Kr (99.998%) were purchased from Matheson. The species were diluted in helium and used without further purification. The initial pH of the liquid in the range from 7 to 14 was set with NaOH and measured with a pH electrode (Cole Parmer). Note that the uptake of acidic gases may alter the initial near-surface pH of the liquid. This effect is taken into account in the data analysis.

Results and Analysis

SO_2(g) Uptake. The SO_2 uptake measurements were conducted entirely with the droplet train flow reactor apparatus. As an example of the data, we show in Figure 2 a plot of $\ln(n_g/n_g')$ as a function of $\bar{c}\Delta A/4F_g$ at pH = 14 and at two temperatures, T = 291 and 273 K. The parameter $\bar{c}\Delta A/4F_g$ is varied by changing both the gas flow rate (F_g) and the droplet surface area (ΔA). Each point is the average of at least 10 area change cycles with error bars representing one standard deviation from the mean in the experimental $\ln(n_g/n_g')$ value. The slope of the plot in Figure 2 yields the value of γ_{meas} (see eq 9). Such plots were generated for the full range of uptake studies. In these studies, the relative change in the trace gas density, $\Delta n_g/n_g$ is typically between 5% and 30%.

SO_2 Uptake as a Function of pH. To display SO_2 data, the uptake is first processed to take gas-phase diffusion into account, as shown in Shi et al.[18] This yields an uptake coefficient γ_0 defined as

$$\frac{1}{\gamma_o} = \frac{1}{\gamma_{meas}} - \frac{1}{\Gamma_{diff}} = \frac{1}{\alpha} + \frac{1}{\Gamma_b} \qquad (10)$$

In Figure 3, the uptake coefficient γ_0 for SO_2 is shown as a function of pH at 283 K and at a gas−liquid interaction time of 5 ms. The SO_2(g) number density was 10^{14} cm^{-3}. Shown also, as open circles, are the previous droplet train flow reactor apparatus results of Jayne et al.[5,24] (adjusted to the same gas−liquid interaction time). The present data are in good agreement with the previous measurements.

At pH less than 2, eq 10 predicts a value of γ_o less than 3×10^{-4}. In fact, the measured value of γ_o (at a 5-ms gas−liquid interaction time) is about 10^{-2}. A set of experiments [including measurements as a function of SO_2(g) density] performed by Jayne et al.[5] indicate that the observed uptake in this pH region is due to a complex formed by SO_2 at the gas−liquid interface. On the millisecond time scale of the droplet experiments, the surface complex rapidly reaches steady state or equilibrium with the gas-phase species and represents a net one-time uptake of a fixed number of molecules, independent of the gas−liquid interaction time (t). For a 5-ms gas−liquid interaction time, γ_0 is measured to be about 10^{-2}.

The onset of an increase in γ_o at pH = 2 is due to the rising solubility via eq 7. In the pH region between about 5 and 10, the uptake is limited by the forward reaction rate k_1 of SO_2 with water (R1), resulting in the observed plateau. Above pH 10, the reaction of SO_2 with OH^- (R2) becomes significant, and γ_o increases once again. The leveling of γ_o for pH > 13 reflects limitation on uptake due to the mass accommodation coefficient α. In this high pH region, uptake is governed mainly by k_2 for the reaction of SO_2 with OH^- and α. (See eqs 8 and 10.)[25]

For SO_2, the parameters k_1, H, and K_{a1} are known.[26,27] They are, at 283 K, $k_1 = 3.4 \times 10^6$ s^{-1}, $H = 2.2$ M atm^{-1}, and $K_{a1} = 1.9 \times 10^{-2}$ M. Values of k_2 and α can be obtained via the global fit to the measured uptake. The solid line in the figure is a best fit to the resistor model, yielding $\alpha = 0.235 \pm 0.022$ and $k_2 = (9.2 \pm 1.4) \times 10^9$ at 283 K. Note that the model curves in Figures 3 and 4 include the effect of an SO_2 surface complex, as discussed above.

The uptake of SO_2(g) significantly affects the droplet surface pH. The treatment of this process is made more complex because, under the conditions of our droplet experiments, equilibrium of the near surface pH is not attained. Therefore, the pH near the surface is time-dependent. To obtain the time-resolved surface pH, one must numerically solve differential equations that include the chemical reaction, liquid-phase diffusion, and mass transport at the interface. This treatment of

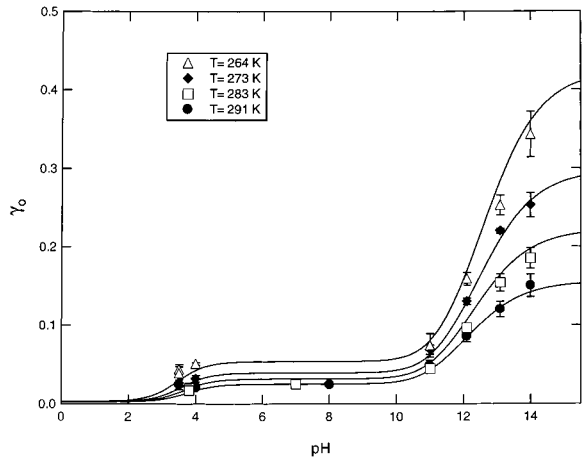

Figure 4. Uptake coefficient γ_o for SO_2 as a function of pH at four droplet temperatures. Gas−droplet contact time $t = 5$ ms and SO_2(g) density $= 10^{14}$ cm^{-3}. The solid lines are the global model fits to the data, with α and k_2 as variables.

surface pH is described in the thesis of Shi (1998)[28] and in Shi et al.[18] (The pH displayed in Figures3 and 4 includes the acidification due to SO_2 uptake.)

SO_2 Uptake as a Function of Temperature. The uptake coefficient γ_o for SO_2 as a function of pH is shown in Figure 4 at four temperatures, $T = 291$, 283, 273, and 264 K. In the data analysis, the parameters H and K_{a1}, as a function of temperature were obtained from Maahs.[27] As is evident, the uptake exhibits a negative temperature dependence. Uptake for pH $\geq$ 4 is governed by reaction (with H_2O for pH < 10 and with OH^- for pH > 10), and the uptake coefficient is proportional to the product $H(D_l k_1)^{1/2}$ (see eq 8). The Henry's law constant has a negative temperature dependence, while the product $(D_l k_1)^{1/2}$ has a smaller positive temperature dependence, giving an overall negative temperature dependence. At the highest pH (~14), the mass accommodation coefficient dominates the uptake, giving a somewhat stronger negative temperature dependence characteristic of α (see eq 12 below).

To obtain values for the mass accommodation coefficient, α, and the rate of the SO_2/OH^- reaction, k_2, the results at all four temperatures were globally fit, using literature values for k_1, H, and K_{a1} obtained from the previously cited sources. The fitting included the expected temperature dependence for k_2 and α. The formulation for k_2, which provided the best global fit to the data in Figure 4, was the diffusion-limited rate coefficient for an ion−neutral molecule reaction obtained from Emerson et al.[29]

$$k_2 = 4\pi P(D_1 + D_2)\sigma N_A/1000 \qquad (11)$$

Here, N_A is Avogadro's number, σ is the effective collision diameter (cm), P is the steric factor, and D_1 and D_2 are the liquid-phase diffusion coefficients of the ion and the neutral molecule, respectively. Liquid-phase diffusion coefficients are commonly expressed in terms of viscosity η as CT/η,[30] where C is a constant that has different values for SO_2 and OH^-. The values of C for SO_2 and OH^- are 3.61×10^{-8} and 1.73×10^{-7}, respectively.[31,32] The values for η were obtained from a fitting to data in CRC Handbook.[33] The factor P was assumed to be unity.

Our previous studies have shown that the mass accommodation coefficient can be expressed as[5]

$$\frac{\alpha}{1-\alpha} = \exp\left(-\frac{\Delta G_{obs}}{RT}\right) \qquad (12)$$

The parameter $\Delta G_{obs} = \Delta H_{obs} - T\Delta S_{obs}$ can be regarded as the Gibbs free energy (with respect to the gas phase) of the transition state between the gas phase and the solvated species. This was the expression used in the global fit of the data shown in Figure 4.

In the global fit, σ and ΔG_{obs} were treated as the unknown parameters. The fitting yielded the effective collision diameter for the SO_2/OH^- reaction as $\sigma = 2.8$ Å and a value for ΔG_{obs} expressed as $\Delta H_{obs} = -7.6 \pm 0.6$ kcal mol^{-1} and $\Delta S_{obs} = -29.2 \pm 2.1$ cal mol^{-1} K^{-1}. The solid lines in Figure 4 are the global model fits to the data with α and k_2 as variables. As is evident, the global fit with these three parameters is in very good agreement with the measurements at all temperatures studied. The model lines at low pH (pH < 2) have included the surface complex, measured by Jayne et al.[5]

The mass accommodation coefficient as a function of temperature is shown in Figure 5. The points in the figure are obtained by extrapolating the experimental data at each temperature to the high-pH plateau limit. The solid line is a calculation on the basis of eq 12, with ΔG_{obs} obtained from the global fit to the model shown in Figure 4.

H_2S(g) Uptake. The magnitude of the H_2S uptake coefficient as a function of pH in the range 1−14 spans the range of the bubble and droplet train flow reactor apparatuses. In the pH region 1−10.6, uptake measurements were conducted with the bubble train reactor apparatus, and from 11 to 14, with the droplet train flow reactor apparatus. In the data analysis, the parameters H and K_{a1}, as functions of temperature, were obtained from DeBruyn et al.[14] and Millero,[34] respectively.

Droplet Train Flow Reactor Apparatus Measurements. The uptake of H_2S by aqueous droplets was measured in the pH range 11−14 at two temperatures, $T = 273$ and 291 K. Detailed measurements were conducted only at these two temperatures because the temperature dependence of the uptake was found to be small.

The H_2S(g) density in these studies was no higher than about 10^{14} cm^{-3}. Calculations show that, in this density range, surface acidification due to H_2S uptake is negligible.[28] Further, the uptake in the pH region studied is principally governed by the rate of H_2S/OH^- reaction. The uptake coefficient is therefore time-independent. These uptake measurements yielded values for the H_2S/OH^- second-order rate coefficient k_2 at $T = 273$ and 291 K (see below).

Bubble Train Reactor Apparatus Measurements. In the pH range 1−10.6, the magnitude of the H_2S uptake is in the region measurable by the horizontal bubble train reactor apparatus. However, the study of H_2S uptake with this apparatus involves an experimental complication. As stated in an earlier section, the gas emerging from the bubble is diluted as the bubble bursts at the exit from the reaction zone. Because of the dilution, the density of the trace gas species in the bubble must be higher than that in the droplet train experiment in order for a detectable signal to be obtained at the mass spectrometer (typically 10^{15} cm^{-3} compared to 10^{13}−10^{14} cm^{-3}). At these higher H_2S densities, the uptake of the species will alter the pH of the near-surface liquid. This, in turn, will affect the uptake in the region where it is pH-dependent. In the bubble train reactor apparatus studies, acidification due to H_2S affects the uptake for initial pH greater than ~6. Below this range, the uptake is independent of pH, being governed by physical Henry's law solubility.

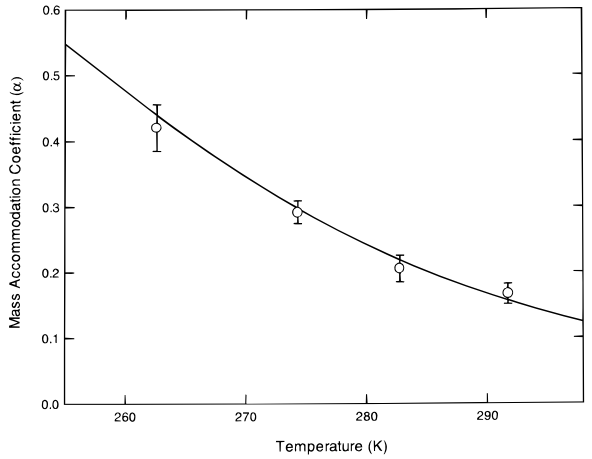

Figure 5. Mass accommodation coefficient, α, for SO_2 as a function of temperature. Solid line is a calculation based on eq 12 with ΔG_{obs} obtained from the global fit to the model shown in Figure 4.

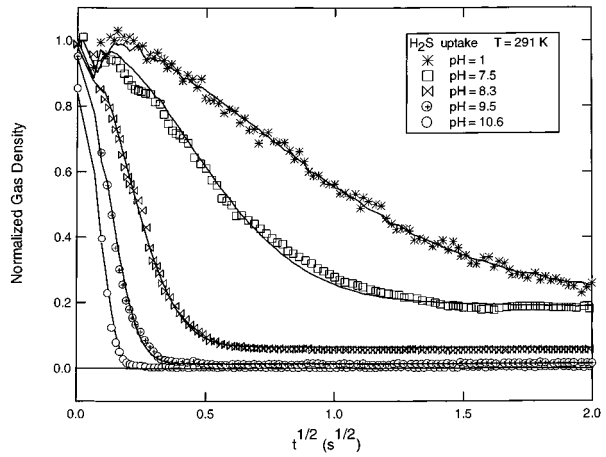

Figure 6. H_2S uptake as a function of the square root of the gas−liquid interaction time at 291 K for pH = 1, 7.5, 8.3, 9.5, and 10.6. Discontinuities in the uptake near $t = 0$ are due to observed pressure changes as the injector enters the liquid.

Because of convective currents induced by the movement of the liquid adjacent to the bubble surface, it is not possible to calculate the surface pH using the method employed in the droplet experiment. Therefore, the effect of near-surface acidification must be treated empirically. At the highest pH studied (pH = 10.6), this was done by varying the H_2S(g) density, which showed that the uptake was density-independent below a H_2S-(g) density of 3×10^{15} cm^{-3}. In the lower pH region 6−10, the effect of H_2S acidification is greater. Here Borax or sodium bicarbonate buffers were used to hold pH at a constant value independent of the H_2S density. The buffer concentration used in these studies was at the lowest value (0.003 M) consistent with holding the pH independent of the H_2S density. Within experimental error, the uptake data obtained with the buffered solutions yielded the same value for the reaction rate coefficient k_2 as was obtained from the low H_2S(g) density and droplet train experiments. As was stated, for pH < 6, uptake is independent of H_2S(g) density.

Typical H_2S uptake data obtained with the horizontal bubble train reactor apparatus are shown in Figure 6 for pH = 1, 7.5, 8.3, 9.5, and 10.6. The normalized density of the gas-phase H_2S is plotted as a function of the square root of the gas−liquid interaction time to emphasize the short-time data where the gas uptake rate is largest. The gas−liquid interaction time was continuously varied from 0 to 4 s as the injector was drawn into the liquid in the reaction tube. Discontinuities in the uptake near $t = 0$ are due to observed pressure changes as the injector enters the liquid. At pH = 1 (see above), the uptake is governed by physical solubility; between pH 7 and 8, the uptake is governed by effective solubility; and at pH > 9, it is determined by the H_2S/OH^- reaction.

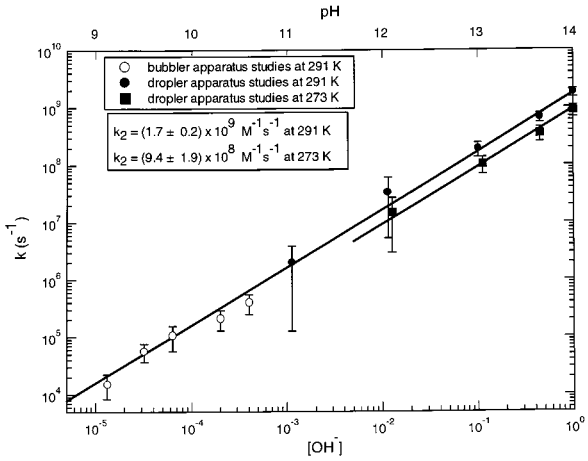

Figure 7. Pseudo-first-order rate coefficient k for the H_2S(aq)/OH^- reaction as a function of [OH^-] at 291 K and 273 K. Data obtained with the bubble train reactor apparatus are shown as open markers, while those measured with the droplet train flow reactor apparatus are shown as solid markers. On the log−log scale, the intercept at [OH^-] = 1 M is the value of k_2, which is $k_2 = (1.7 \pm 0.2) \times 10^9$ M^{-1} s^{-1} at 291 K and $(9.4 \pm 1.9) \times 10^8$ M^{-1} s^{-1} at 273 K.

As was pointed out above, in general, the uptake of H_2S is a function of the solubility parameter H, K_{a1}, the liquid-phase diffusion coefficient D_l, the mass accommodation coefficient α, and the rate coefficients k_1 and k_2. The value of K_{a1} is known and D_l can be estimated using the cubic cell model.[31] At 291 K, these parameters are $K_{a1} = 9.1 \times 10^{-8}$ M and $D_l = 1.4 \times 10^{-5}$ cm^2 s^{-1}. The rate coefficients k_1 and k_2 have not previously been measured and will be evaluated using the nonlinear least-squares model fit to the data which yields the pseudo-first-order rate coefficient $k = (k_1 + k_2[OH^-])$. The value of H has been previously measured by Wilhelm et al.[35] and Edwards et al.[36] as 0.12 M atm^{-1} and by De Bruyn et al.[14] as 0.10 M atm^{-1} at 291 K. However, in this study, H will be evaluated again independently. The solid lines in Figure 6 are the nonlinear least-squares fits to the data using the model described in Swartz et al.[23]

The numerical fit of the experimental data to the model yields the value for the Henry's coefficient at 291 K of $H = 0.11 \pm .01$ M atm^{-1}, which is in good agreement with the previously measured values of H. A global fit to all of the data as a function of pH indicates that k_1 is less than 10^4 s^{-1}. In other words, the hydrolysis channel for the reaction of H_2S (R3) does not play a significant role in the uptake process, that is, $k = k_2[OH^-]$ (see eq 8). Further, even at the highest pH studied (pH = 14 with the droplet train flow reactor apparatus), the uptake continues to rise and evidently is not yet limited by α. (This is shown in Figure 11, described below.) The H_2S uptake data, therefore, yield only a lower limit of $\alpha > 4 \times 10^{-2}$ at 291 K.

In Figure 7, we plot, on a log−log scale, k [the pseudo-first-order reaction-rate coefficient for H_2S(aq) with OH^-] as a function of [OH^-] at 291 and 273 K. The data obtained with the bubble train reactor apparatus are shown as open markers, while those measured with the droplet train flow apparatus are shown as solid markers. In this way of displaying the data, the intercept at pH = 14 ([OH^-] = 1 M) is k_2. The figure yields $k_2 = (1.7 \pm 0.2) \times 10^9$ M^{-1} s^{-1} at 291 K. This is roughly an

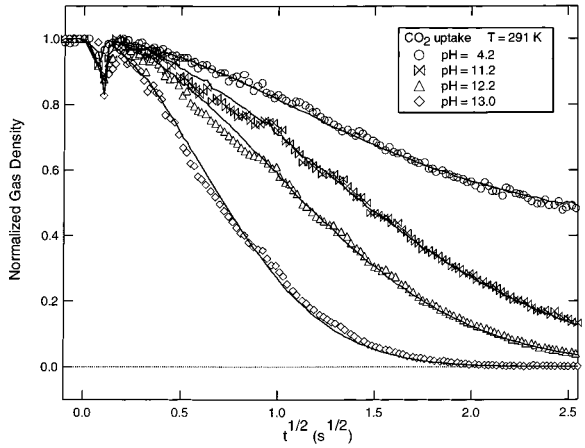

Figure 8. CO_2 uptake at 291 K as a function of square root of the gas−liquid interaction time at pH = 4.2, 11.2, 12.2, and 13.

order of magnitude smaller than the diffusion-limited value, which is estimated to be $\sim 2.5 \times 10^{10}$ M^{-1} s^{-1} at $T = 291$ K.[29,37]

Droplet uptake studies were also conducted at $T = 273$ K (see Figure 7). At this temperature, the data yielded $k_2 = (9.4 \pm 1.9) \times 10^8$ M^{-1} s^{-1}. The temperature dependence is consistent with an activation energy $\Delta E \sim 5$ kcal/mol (assuming a simple Arrhenius form).

CO_2(g) Uptake. Because of the low Henry's law coefficient of CO_2 ($H = 4 \times 10^{-2}$ M atm^{-1} at 291 K),[33] its uptake is below the sensitivity of the droplet train flow reactor apparatus, even with the highest-pH droplets, which contain 3 M NaOH. The lower limit of the uptake coefficient measurable with the droplet train flow reactor apparatus is about 10^{-3}, which implies $k < 3 \times 10^5$ s^{-1}. With 3 M NaOH, this corresponds to a rate coefficient for the reaction with OH^- of $k_2 < 10^6$ M^{-1} s^{-1}. The magnitude of the uptake coefficient, however, falls into the optimal measurement range of the horizontal bubble train reactor apparatus. The uptake of CO_2 was measured with the bubble reactor train apparatus in the pH range 2.8−13, at three temperatures, 291, 283, and 275 K. The basic solutions were prepared by adding NaOH to water purified in a Milli-Q system. Calculations show that dissolved CO_2 does not significantly alter the near surface pH of the basic solutions studied.

Typical CO_2 uptake data are shown in Figure 8 for pH = 4.2, 11.2, 12.2, and 13 at 291 K. As is evident, uptake of CO_2 is lower than that of H_2S under similar pH conditions. A fit of the data to the numerical model,[23] with $H = 4 \times 10^{-2}$ M atm^{-1}, $K_{a1} = 4 \times 10^{-7}$, and an estimated $D_l = 1.26 \times 10^{-5}$ cm^2 s^{-1}, yields a second-order rate coefficient for the CO_2/OH^- reaction of $k_2 = (4.0 \pm 0.5) \times 10^3$ M^{-1} s^{-1}. For the analysis of data at the other two temperatures, the parameters H and K_{a1}, as functions of temperature, were obtained from CRC Handbook[33] and Perrin,[38] respectively.

In Figure 9, we plot, on a log−log scale, k [the pseudo-first-order reaction-rate coefficient for CO_2(aq) with OH^-] as a function of [OH^-] at 291 and 275 K. The solid squares represent the data taken at 291 K, and the open circles represent that taken at 275 K. To simplify the presentation, results obtained at 283K are not shown. As was the case with H_2S, the effect of hydrolysis (k_1) on the CO_2 uptake is not observed. The slope of these plots yields k_2. The values of the second-order coefficients for the CO_2/OH^- reaction measured in this study are, at 291 K, $k_2 = (4.0 \pm 0.7) \times 10^3$ M^{-1} s^{-1} (as stated above); at 283 K, $k_2 = (3.0 \pm 0.9) \times 10^3$ M^{-1} s^{-1}; and at 275 K, $k_2 = (1.9 \pm 0.8) \times 10^3$ M^{-1} s^{-1}.

The literature contains several rate coefficient measurements for the CO_2/OH^- reaction. Sirs[15] summarized and evaluated the

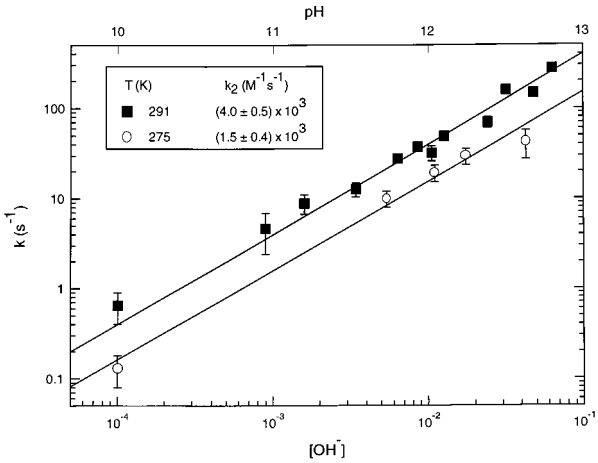

Figure 9. Pseudo-first-order rate coefficient k for the CO_2(aq)/OH^- reaction as a function of [OH^-] at 291 K. On the log−log plot, the intercept at [OH^-] = 1 M is the value of k_2, which is $(4.0 \pm 0.7) \times 10^3$ at 291 K and $(1.9 \pm 0.8) \times 10^3$ at 273 K.

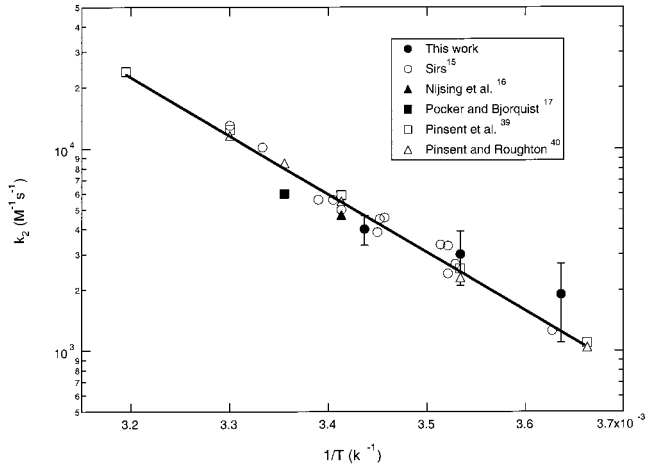

Figure 10. Values of log k_2 for the CO_2/OH^- reaction from this and several other studies are plotted as a function of $1/T$. The solid line is a fit to the earlier data.

literature values up to about 1957. Two other measurements were performed subsequently.[16,17] Figure 10 brings together values of k_2 from this work and from several other studies.[15−17,39,40] The display is in the form log k_2 vs $1/T$. The solid line is a fit to the earlier data provided by Sirs.[15] It is evident that our measured rate coefficients at the three temperatures are consistent with the previous studies.

Experimental Precision. The error bars in this work represent 1σ precision of the results obtained from fitting the experimental data. The bubble train apparatus has been calibrated using known values of solubility constants and reaction rates. The calibrations were consistent with the uncertainties quoted in this work (about 20%). The results from the droplet train apparatus were also compared to literature values, and here again, the results were consistent with the uncertainties quoted in this work.

Discussion

Uptake of the Three Species: A Comparison. The uptake coefficients γ_o for the three species, as a function of pH at 291 K, are displayed in Figure 11. Shown also, as solid triangles, are the previous droplet train flow reactor apparatus results of Jayne et al.[5] (adjusted to the same temperature and gas−liquid interaction time). The uptake coefficients are plotted on a log scale to span the 5 orders of magnitude required to display γ_o

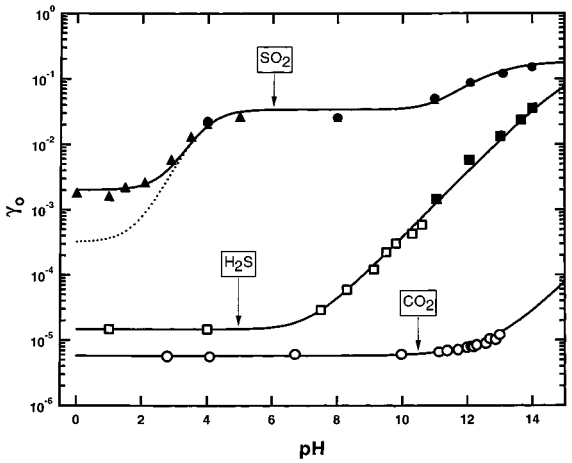

Figure 11. Summary plot of uptake coefficients for SO_2, H_2S, and CO_2 as a function of pH measured with the droplet train flow reactor apparatus (solid markers) and the horizontal bubble train reactor apparatus (open markers). The dotted line is predicted SO_2 uptake without the SO_2 surface complex. The data obtained with the droplet train flow reactor are for a gas−liquid interaction time of 5 ms.

for the three species. In the droplet experiments, γ_o is obtained directly from measurements, via eqs 9 and 4. In Figure 11 (as in Figures 3 and 4), the droplet results shown are for a gas−liquid contact time (t) of 5 ms. The γ_o values for bubble train results are calculated at each pH from eqs 8 and 10, using H and k_2 values obtained from model fits to the experimental uptake data at that pH. In calculating the solubility uptake parameter Γ_{sol}, the gas−liquid contact time was set at 5 ms so that the droplet and bubble train results could be compared. For clarity, error bars have been omitted from this display. The solid lines in the figure are model calculations using parameters obtained in the present study, as discussed above. The dotted line is the predicted SO_2 uptake, which does not include the presence of the SO_2 surface complex. The principal parameters governing the species uptake are listed in Table 1.

Of the three gases, the uptake of SO_2 is highest, primarily because of its greater solubility (H) and rate coefficient k_2 (see Table 1). At pH 14, the SO_2 uptake is governed by mass accommodation. On the other hand, at this pH, CO_2 and H_2S uptake are controlled by their reaction with OH^-. The H_2S uptake data yield only a lower limit of α at pH = 14. In the pH region 4−10, the SO_2 uptake is at a pH-independent plateau where γ_o is governed by the reaction of SO_2(aq) with H_2O. As noted above, the hydrolysis reactions of H_2S and CO_2 are not observed to affect the uptake process. The upper limits for the reaction-rate coefficients of H_2S and CO_2 with water are 1×10^4 s^{-1} and 0.1 s^{-1}, respectively. The latter limit is consistent with the literature value of 0.014 s^{-1} at 291 K.[39] The pH-independent plateaus in the uptake of these two species are due to uptake governed by Henry's law physical solubility.

There is evidence in the SO_2 uptake data at low pH for the formation of a surface complex, consistent with a number of recent experimental and theoretical investigations.[41] This complex has a measurable effect on the uptake only in the low-pH region where γ_0 is relatively small (<0.002). The SO_2 uptake at higher pH and the uptake of H_2S and CO_2 do not show evidence for interfacial reactions and are entirely in accord with bulk-phase processes. In the case of SO_2, new uptake measurements at high pH have distinguished k_2 and α, clarifying earlier interpretation of surface reaction at pH > 10 (Jayne et al.[5])

Reactions of the Three Species with OH^-. The three molecules SO_2, H_2S, and CO_2 are all acidic in aqueous solution, and they all react with OH^-. The rate coefficients for the reactions of these three species with OH^- (and, as appropriate, H_2O) are shown in Table 1. The reaction-rate coefficients for SO_2 and CO_2 reacting with OH^- span nearly 6 orders of magnitude. On the other hand, molecular beam experiments of CO_2 and SO_2 reacting with hydrated OH^- clusters containing one to three H_2O molecules,[42] showed that the reaction cross section of SO_2 is only three times larger than the reaction cross section of CO_2. Thus, the large difference between the aqueous reaction rates with OH^- for the two species is somewhat surprising. Molecular beam experiments further showed that the CO_2 and SO_2 reaction with OH^- was initiated by the formation of a complex with at least one H_2O molecule.

We suggest that the reaction of CO_2 with OH^- in aqueous solutions, is limited by the rate of formation of the $CO_2(H_2O)_n$ complex, which is expected to be low because CO_2 does not possess a permanent dipole moment. On the other hand, SO_2 does possess a permanent dipole moment, which enhances the rate of formation of $SO_2(H_2O)_n$ complex. Because H_2S also possesses a permanent dipole moment, the reaction rate of H_2S with OH^- is expected to be large, closer to that of the SO_2/OH^- reaction rate, which, in fact, is the case.

Atmospheric Implications. In the absence of Henry's law saturation, mass transport of SO_2 into atmospheric aerosols is a function of the mass accommodation coefficient, α, and the gas-phase diffusion coefficient (Γ_{diff}). The parameter α is rate limiting when $\alpha < \Gamma_{diff}$. The mass accommodation coefficient α for SO_2 was measured to be in the range 0.175−0.39, depending on droplet temperature. The magnitude of Γ_{diff} depends on the size of the droplet and the ambient pressure. For SO_2 at a total pressure of 760 Torr, Γ_{diff} is larger than 0.2 for aerosols with diameters less than 1μm. A significant fraction of tropospheric aerosols is in this size range. Therefore, realistic modeling of SO_2−aerosol interactions should utilize measured values of the mass accommodation coefficient. In the absence of a reactive sink, partitioning of SO_2 between the liquid and gas phases is determined by the effective Henry's law constant.

Hydrogen sulfide and carbon dioxide are relatively insoluble gases. Under typical atmospheric conditions, uptake of H_2S and CO_2 by cloud droplets at pH < 7 is governed by solubility. However, the air−sea exchange rate for H_2S and CO_2 will be governed by their reactions with OH^- when the ocean surface is stirred by high-speed winds.[43] In this case, the measured rate coefficients for reaction with OH^- should be used in modeling ocean uptake process.

Acknowledgment. We thank Dr. Leah R. Williams for helpful discussions. Funding for this work was provided by the National Science Foundation, Grants ATM-93-10407 and ATM-96-32599, the U.S. Environmental Protection Agency, Grant R-821256-01-0, and the Department of Energy, Grants DE-FG02-91ER61208 and DE-FG02-94ER61854.

References and Notes

(1) Barrie, L. A. *J. Geophys. Res.* **1985**, *90*, 5789.
(2) Watts, S. F. *Atmos. Environ.* **2000**, *34*, 761.
(3) Warneck, P. *Chemistry of the Natural Atmosphere*; International Geophysics Series; Academic Press: San Diego, CA, 1988; Vol. 41, p 493.
(4) Hoigne, J.; Bader, H.; Haag, W. R.; Staehelin, J. *Water Res.* **1985**, *19* (8), 993.
(5) Jayne, J. T.; Davidovits, P.; Worsnop, D. R.; Zahniser, M. S.; Kolb, C. E. *J. Phys. Chem.* **1990**, *94*, 6041.
(6) Hanson, D. R.; Ravishankara, A. R. *J. Phys. Chem.* **1993**, *97*, 12309.
(7) George, Ch.; Behnke, W.; Scheer, V.; Zetzsch, C.; Magi, L.; Ponche, J. L.; Mirabel, Ph. *Geophs. Res. Lett.* **1995,** *22*, 1505.
(8) Hu, J. H.; Shi, Q.; Davidovits, P.; Worsnop, D. R.; Zahniser, M. S.; Kolb, C. E. *J. Phys. Chem.* **1995**, *99*, 8768.

(9) Swartz, E.; Shi, Q.; Davidovits, P.; Jayne; J. T.; Worsnop; D. R.; Kolb, C. E. *J. Phy. Chem. A* **1999**, *103* (44), 8824.

(10) Tang, I. N.; Lee, J. H. *The Chemistry of Acid Rain: Sources and Atmospheric Processes*; Johnson, R. W., Gordon, G. E., Eds.; ACS Symposium Series No. 349; American Chemical Society: Washington, D.C., 1987; p 109.

(11) Worsnop, D. R.; Zahniser, M. K.; Kolb, C. E.; Gardner, J. A.; Watson, L. R.; Van Doren, J. M.; Jayne, J. T.; Davidovits, P. *J. Phys. Chem.* **1989**, *93*, 1159.

(12) Ponche, J. L.; George, Ch.; Mirabel, Ph. *J. Atmos. Chem.* **1993**, *16*, 1.

(13) Shimono, A.; Koda, S. *J. Phys. Chem*. **1996**, *100*, 10269.

(14) De Bruyn, W. J.; Swartz, E.; Hu, J. H.; Shorter, J. A.; Davidovits, P.; Worsnop, D. R.; Zahniser, M. S.; Kolb, C. E. *J. Geosphy. Res.* **1995,** *100*, 7245.

(15) Sirs, J. A. *Trans. Faraday Soc*. **1958**, *54*, 201.

(16) Nijsing, R. A. T. O.; Hendriksz, R. H.; Kramers, H. *Chem. Eng. Sci.* **1959**, *10*, 88.

(17) Pocker Y.; Bjorkquist, D. W. *J. Am. Chem. Soc*. **1977**, *99* (20), 6537.

(18) Shi, Q.; Davidovits, P.; Jayne; J. T.; Worsnop; D. R.; Kolb C. E. *J. Phy. Chem. A* **1999**, *103* (44), 8812.

(19) Fuchs, N. A.; Sutugin, A. G. *Highly Dispersed Aerosols*; Ann Arbor Science Publishers: Ann Arbor, MI, 1970.

(20) Schwartz, S. E. *Chemistry of Multiphase Atmospheric Systems*; Jaeschke, W., Ed.; NATO ASI Series; Springer-Verlag: Berlin, 1986; Vol. G6, p 415.

(21) Danckwerts, P. V. *Trans. Faraday Soc.* **1951,** *47*, 1014.

(22) Robinson, G. N.; Worsnop, D. R.; Jayne, J. T.; Kolb, C. E.; Davidovits, P. *J. Geophys. Res.* **1997**, *102*, 3583.

(23) Swartz, E.; Boniface, J.; Techertkov, I.; Rattigan, O. V.; Robinson, D. V.; Davidovits, P.; Jayne, J. T.; Worsnop, D. R.; Kolb, C. E. *Environ. Sci. Technol.* **1997**, *31*, 2634.

(24) In the original analysis, the surface pH was assumed to be at the equilibrium value, which overestimates the surface acidification. These results have been reanalyzed, and the pH shown is the actual near-surface pH calculated using the numerical model described in Shi et al. (ref 18).

(25) This analysis differs from the previous measurements for pH ≤ 11.5 (ref 5), which, as stated earlier, were erroneously interpreted as evidence for a surface reaction uptake channel at high pH. The new results presented here clearly indicates that enhanced uptake observed for pH > 10 is due to the bulk reaction of dissolved SO_2 with OH^-.

(26) Eigen, M.; Kustin, K.; Maass, G. Z. *Phys. Chem. (Munich)* **1961**, *30*, 130.

(27) Maahs, H. G. *Heterogeneous Atmospheric Chemistry*; Schryer, D. R., Ed.; Geophysical Monograph No. 26; American Geophysical Union: Washington, D.C., 1982; p 187.

(28) Shi, Q. Ph.D. Thesis, Chemistry Department, Boston College, Boston, MA, 1998.

(29) Emerson, M. T.; Grunwald, E.; Kromhout, R. A. *J. Chem. Phys.* **1960**, *33* (2), 547.

(30) Reid, R. C.; Prausnitz, J. M.; Poling, B. E. *The Properties of Gases and Liquids*, 4th ed.; McGraw-Hill: New York, 1987.

(31) Houghton G. *J. Chem. Phys.* **1964**, *40* (6), 1628.

(32) Leaist, D. G. *J. Phys. Chem*. **1987,** *91*, 4635.

(33) *Handbook of Chemistry and Physics*, 73rd ed.; Lide, D. R., Ed.; CRC Press: Boca Raton, FL, 1992; pp 6-3 and 6-10.

(34) Millero, F. J. *Mar. Chem.* **1986**, *18*, 121.

(35) Wilhelm, E.; Battino, R.; Wilcock, R. J. *Chem Rev*. **1977**, *77*, 219.

(36) Edwards, T. J.; Maurer, G.; Newman, J.; Prausnitz, J. M. *AIChE J*. **1978**, *24*, 966.

(37) Albert, R. A.; Silbey, R. J. *Physical Chemistry*; John Wiley & Sons: New York, 1992; p 721.

(38) Perrin, D. D. *Ionisation Constants of Inorganic Acids and Bases in Aqueous Solution*; IUPAC Chemical Data Series No.29; Pergamon Press: Oxford, U.K., 1982; p 20.

(39) Pinsent, B. R. W.; Pearson, L.; Roughton, F. J. W. *Trans. Faraday Soc*. **1956**, *52*, 1512.

(40) Pinsent, B. R. W.; Roughton, F. J. W. *Trans. Faraday Soc.* **1951,** *47*, 263.

(41) Donaldson, D. J.; Guest, J. A.; Goh, M. C. *J. Phys. Chem*. **1995**, *99*, 9313. Bishendon, E.; Donaldson, D. J. *J. Phys. Chem*. **1998**, *102*, 4638. Donaldson, D. J.; Anderson, D. *J. Phys. Chem*. **1999**, *103*, 871.

(42) Hierl, P. M.; Paulson, J. F. *J. Chem. Phys.* **1984**, *80* (10), 4890.

(43) Hoover, T. E.; Berkshire, D. C. *J. Geophys. Res*. **1969**, *74*, 456.